

Modelling Vegetation and the Carbon Cycle as Interactive Elements of the Climate System

Hadley Centre technical note 23

**Peter M. Cox, *Richard A. Betts, *Chris D. Jones
*Steven A. Spall, **Ian J. Totterdell*

**Hadley Centre, Met Office, Bracknell, Berks RG12 2SY, UK*

***Southampton Oceanography Centre, Southampton SO14 3ZH, UK*

15 January 2001



Modelling Vegetation and the Carbon Cycle as Interactive Elements of the Climate System

[△]Peter M. Cox, [△]Richard A. Betts, [△]Chris D. Jones,
[△]Steven A. Spall, [○]Ian J. Totterdell

[△] Hadley Centre, Met Office, Bracknell, Berks RG12 2SY, UK
[○] Southampton Oceanography Centre, Southampton SO14 3ZH, UK

January 15, 2001

To appear in the Proceedings of the RMS Millenium Conference

Abstract

The climate system and the global carbon cycle are tightly coupled. Atmospheric carbon in the form of the radiatively active gases, carbon dioxide and methane, plays a major role in the natural greenhouse effect. The continued increase in the atmospheric concentrations of these gases, due to human emissions, is predicted to lead to significant climatic change over the next 100 years. The best estimates suggest that more than half of the current anthropogenic emissions of carbon dioxide are being absorbed by the ocean and by land ecosystems (Schimel *et al* (1996)). In both cases the processes involved are sensitive to the climatic conditions. Temperature affects the solubility of carbon dioxide in sea-water and the rate of terrestrial and oceanic biological processes. In addition, vegetation is known to respond directly to increased atmospheric CO₂ through increased photosynthesis and reduced transpiration (Sellers *et al* (1996a), Field *et al* (1995)), and may also change its structure and distribution in response to any associated climate change (Betts *et al* (1997)). Thus there is great potential for the biosphere to produce a feedback on the climatic change due to given human emissions.

Despite this, simulations carried out with General Circulation Models (GCMs) have generally neglected the coupling between the climate and the biosphere. Instead, vegetation distributions have been static and atmospheric concentrations of CO₂ have been prescribed based on results from simple carbon cycle models, which neglect the effects of climate change (Enting *et al* (1994)). This paper describes the inclusion of vegetation and the carbon cycle as interactive elements in a GCM. The coupled climate-carbon cycle model is able to reproduce key aspects of the observations, including the global distribution of vegetation types, seasonal and zonal variations in ocean primary production, and the interannual variability in atmospheric CO₂. A transient simulation carried out with this model suggests that previously neglected climate-carbon cycle feedbacks could significantly accelerate atmospheric CO₂ rise and climate change over the 21st century (Cox *et al* (2000)).

1 Introduction

The biosphere influences weather and climate over an extraordinary range of timescales (see table 1). Stomatal pores on plant leaves respond to the environment with a characteristic timescale of minutes, modifying evapotranspiration and producing detectable impacts on the diurnal evolution of the boundary layer and near-surface variables. At the other extreme, deep-rooted plants and soil microbes together amplify the concentration of carbon dioxide in the soil, possibly accelerating the weathering of silicate rocks which is believed to control the concentration of atmospheric CO₂ on geological timescales (Lovelock and Kump (1994), Berner (1997)). In between are processes operating over decades to centuries which have great relevance to the issue of human-induced climate change.

Key amongst these is the uptake of CO₂ by the oceans and by land ecosystems, which are together responsible for absorbing more than half of the current human CO₂ emissions (Schimel *et al* (1996)). Marine biota modify oceanic uptake by producing carbonate shells which sink to depth, producing a biological carbon pump. The photosynthetic rates of land plants are enhanced under high CO₂, which acts to increase carbon storage in vegetation and soils.

However, the atmosphere-ocean and atmosphere-land exchanges of carbon are also known to be sensitive to climate. Warming reduces the solubility of carbon dioxide in sea-water, and increases soil and plant respiration. As a result, climate warming alone may result in a reduction of carbon storage. The competition between the direct effects of increasing CO₂ (which tends to increase carbon storage in the ocean and on land), and the effects of any associated climate warming (which may reduce carbon storage, especially on land), currently seems to favour CO₂ uptake, but how might this change in the future?

To address this question we have included dynamic vegetation and an interactive carbon cycle in the Hadley Centre GCM. The structure of the coupled climate-carbon cycle model is described in section 2, and its pre-industrial simulation is analysed in section 3. Results from the first transient climate change simulation are presented in section 4. Finally, the associated uncertainties and implications are discussed in section 5.

2 Model Description

The model used here (“HadCM3LC”) is a coupled ocean-atmosphere GCM with an interactive carbon cycle and dynamic vegetation. Figure 1 is a schematic showing the coupling of these components, and the new feedbacks which have been introduced.

a Ocean-Atmosphere GCM (HadCM3L)

The ocean-atmosphere GCM is based on the 3rd generation Hadley Centre coupled model, “HadCM3” (Gordon *et al* (2000)), which is one of the first 3-D OAGCMs to be used predictively without flux adjustments. This advance was achieved partly through improved treatments of atmospheric processes and subgrid ocean transports (Gent and McWilliams (1990)), but was primarily a result of the use of an enhanced ocean horizontal resolution of 1.25° latitude by 1.25° longitude. The additional computational expense of including an interactive carbon cycle made it necessary to reduce the ocean resolution to that used in the 2nd generation Hadley Centre model (Johns *et al* (1997)). Thus, the model used here has a horizontal resolution for both atmosphere and ocean of 2.5° latitude by 3.75° longitude, with 19 vertical levels in the atmosphere and 20 in the ocean. The atmospheric physics and dynamics packages are identical to those used in HadCM3 (Pope *et al* (2000)), including a new radiation scheme (Edwards and Slingo (1996)), a parametrization of momentum by convective processes (Kershaw and Gregory (1997)), and an improved land surface scheme that simulates the effects of soil water phase change and CO₂-induced stomatal closure (Cox *et al* (1999)). The reduced ocean resolution required some modification to the diffusion coefficients (Gent and McWilliams (1990)) and to the parametrization of Mediterranean outflow, but otherwise the ocean physics is as described by Gordon *et al* (2000).

HadCM3L was tested initially without flux adjustments, but the resulting errors in the climate simulation were found to have unacceptably large impacts on offline simulations of the land and ocean carbon cycles. It was therefore decided to use flux adjustments for this first series of coupled climate-carbon cycle experiments.

b The Hadley Centre Ocean Carbon Cycle Model, HadOCC

The ocean is a significant sink for anthropogenic carbon dioxide, with the suggestion that a third of anthropogenic emissions of CO₂ are taken up by the ocean (Siegenthaler and Sarmiento (1993)). Surface waters exchange CO₂ with the atmosphere, but it is the transfer of CO₂ to depth that determines

the capacity of the ocean for long-term uptake. There are several mechanisms for this transfer of CO₂ to deeper waters.

Phytoplankton, the plants of the ocean ecosystem, take up CO₂ during their growth, converting the carbon to organic forms. The sinking of a fraction of this organic carbon is a mechanism for the export of carbon to depth, where it is remineralised back to CO₂. This process is known as the biological pump. Reproducing primary production (growth of phytoplankton) and the export of organic carbon is important if a model is to represent the fate of CO₂ in the ocean.

The Met Office ocean model has already been used in the estimate of oceanic uptake of anthropogenic CO₂ (Taylor (1995)). This model included only inorganic cycling of carbon, in which a solubility pump acts to increase the deep ocean carbon concentration. Carbon dioxide is absorbed in cold, dense polar waters which sink to the deep ocean. Equatorial upwelling allows deep waters to warm and release carbon dioxide back to the atmosphere. The simulations were found to be useful in studying carbon uptake, but it was noted that the neglect of ocean biology led to some unrealistic results such as the incorrect phase of seasonal variations in partial pressure at high latitudes. Ocean biology was added to the carbon model in order to improve the simulation of carbon uptake and to increase the range of possible simulated responses to scenarios of climate change (Palmer and Totterdell (in press)).

The resulting model, "HadOCC" (Hadley Centre Ocean Carbon Cycle model), simulates the movements of carbon within the ocean system, including exchange of carbon dioxide gas with the atmosphere, the circulation of dissolved inorganic carbon (known as DIC or tCO₂) within the ocean, and the cycling of carbon by the marine biota. The principle components of the model are handled as tracers within the physical ocean model. They are: (nitrogenous) nutrient, phytoplankton, zooplankton, detritus, tCO₂ and alkalinity.

The air-to-sea flux of carbon dioxide is calculated using standard parametrizations:

$$F_{AS} = K (c_a - c_o) \quad (1)$$

where c_a and c_o are respectively the partial pressures of CO₂ in the atmosphere and ocean at a given location. K parametrizes the effect of the wind speed on the gas transfer velocity, using the formulation of Wanninkhof (1992). Winds are obtained from the atmospheric model. The partial pressure of CO₂ in the surface waters is determined by solving equations representing the sea water acid-base system. The expressions for the dissociation constants of carbonic acid, hydrogen carbonate, boric acid and water and for the solubility of CO₂ in seawater are taken from DOE (1994). Using the salinity dependent boron concentration of Peng (1987), the acid base system is solved using the method of Bacastow and Keeling (1981) to yield the concentration of carbonic acid and hence the partial pressure of CO₂. The temperature and salinity values used in these calculations are the local values from the ocean model.

The biological model is an explicit ecosystem model consisting of the four components; nutrient (assumed to be nitrate), phytoplankton, zooplankton and (sinking) detritus. The complexity of the model was restricted to just four compartments in order for it to be economical enough for use in long integrations. This means that the behaviours of many different species and size-fractions are aggregated into a single component for each of phytoplankton and zooplankton. The model calculates the flow of nitrogen between the four components of the ecosystem at each grid box, and also computes the associated transfers of carbon and alkalinity. The carbon flows have no direct effect on the behaviour of the ecosystem as growth of phytoplankton is not limited by availability of carbon.

The phytoplankton population changes as a result of the balance between growth, which is controlled by light level and the local concentration of nutrient, and mortality, which is mostly as a result of grazing by zooplankton. Detritus, which is formed by zooplankton excretion and by phyto- and zooplankton mortality, sinks at a fixed rate and slowly remineralises to reform nutrient and dissolved inorganic carbon. Thus both nutrient and carbon are absorbed by phytoplankton near the ocean surface, pass up the food chain to zooplankton, and are eventually remineralised from detritus in the deeper ocean.

Over the last decade a number of groups have developed equilibrium biogeography models which successfully predict the global distribution of vegetation based on climate (Prentice *et al* (1992), Woodward *et al* (1995)). Such models have been coupled “asynchronously” to GCMs in order to quantify climate-vegetation feedbacks. This involves an iterative procedure in which the GCM calculates the climate implied by a given land-cover, and the vegetation model calculates the land-cover implied by a given climate. The process is repeated until a mutual climate-vegetation equilibrium is reached (Claussen (1996), Betts *et al* (1997)). Such techniques have yielded interesting results, but are not appropriate for simulating transient climate change for which the terrestrial biosphere may be far from an equilibrium state.

In order to fully understand the role of climate-vegetation feedbacks on these timescales we need to treat the land-cover as a interactive element, by incorporating dynamic global vegetation models (DGVMs) within climate models. The earliest DGVMs were based on bottom-up “gap” forest models, which explicitly model the growth, death and competition of individual plants (Friend *et al* (1993), Post and Pastor (1996)). Such models can produce very detailed predictions of vegetation responses to climate, but they are computationally expensive for large-scale applications. Also, GCM climates are not likely to be sensitive to the details of the species or age composition of the land-cover. For this study it is more appropriate to adopt a “top-down” DGVM approach, in which the relevant land-surface characteristics, such as vegetated fraction and leaf area index, are modelled directly (Foley *et al* (1996)). A model of this type, called “TRIFFID” (“Top-down Representation of Interactive Foliage and Flora Including Dynamics”), has been developed at the Hadley Centre for use in these coupled climate-carbon cycle simulations.

TRIFFID defines the state of the terrestrial biosphere in terms of the soil carbon, and the structure and coverage of five plant functional types (Broadleaf tree, Needleleaf tree, C₃ grass, C₄ grass and shrub) within each model gridbox. The areal coverage, leaf area index and canopy height of each type are updated based on a carbon balance approach, in which vegetation change is driven by net carbon fluxes calculated within the “MOSES 2” land surface scheme. MOSES 2 is a tiled version of the land surface scheme described by Cox *et al* (1999), in which a separate surface flux and temperature is calculated for each of the land-cover types present in a GCM gridbox. In its standard configuration, MOSES 2 recognises the five TRIFFID vegetation types plus four non-vegetation land-cover types (bare soil, inland water, urban areas and land ice). Carbon fluxes for each of the vegetation types are derived using the coupled photosynthesis-stomatal conductance model developed by Cox *et al* (1998), which utilises existing models of leaf-level photosynthesis in C₃ and C₄ plants (Collatz *et al* (1991), Collatz *et al* (1992)). Plant respiration is broken-down into a growth component, which is proportional to the photosynthetic rate, and a maintenance component which is assumed to increase exponentially with temperature ($q_{10} = 2$). The resulting rates of photosynthesis and plant respiration are dependent on both climate and atmospheric CO₂ concentration. Therefore, with this carbon-balance approach, the response of vegetation to climate occurs via climate-induced changes in the vegetation to atmosphere fluxes of carbon.

Figure 2 is a schematic showing how the MOSES 2 land-surface scheme is coupled to TRIFFID for each vegetation type. The land-atmosphere fluxes (above the dotted line) are calculated within MOSES 2 on every 30 minute GCM timestep and time-averaged before being passed to TRIFFID (usually every 10 days). TRIFFID (below the dotted line of figure 2) allocates the average net primary productivity over this coupling period into the growth of the existing vegetation (leaf, root and wood biomass), and to the expansion of the vegetated area in each gridbox. Leaf phenology (bud-burst and leaf drop) is updated on an intermediate timescale of 1 day, using accumulated temperature-dependent leaf turnover rates. After each call to TRIFFID the land surface parameters required by MOSES 2 (e.g. albedo, roughness length) are updated based on the new vegetation state, so that changes in the biophysical properties of the land surface, as well as changes in terrestrial carbon, feedback onto the atmosphere (see figure 1). The land surface parameters are calculated as a function of the type, height and leaf area index of the vegetation.

The natural land-cover evolves dynamically based on competition between the types, which is modelled using a Lotka-Volterra approach and a (tree-shrub-grass) dominance hierarchy. We also prescribe some agricultural regions, in which grasslands are assumed to be dominant. Carbon lost from the vegetation as a result of local litterfall or large-scale disturbance, is transferred into a soil carbon pool, where it is broken down by microorganisms which return CO_2 to the atmosphere. The soil respiration rate is assumed to double for every 10 K warming (Raich and Schlesinger (1992)), and is also dependent on the soil moisture content in the manner described by McGuire *et al* (1992).

3 Preindustrial State

a Spin-up Methodology

The present day natural carbon sink of about 4 GtC yr^{-1} is a small fraction of the gross carbon exchanges between the Earth’s surface and the atmosphere. It is therefore vitally important to reach a good approximation to a pre-industrial equilibrium, since even a small model drift could easily swamp this signal in a climate change experiment. With this in mind, a spin-up methodology was designed to obtain a carbon cycle equilibrium to within $\pm 10\%$ of the current natural carbon sink (i.e. $\pm 0.4 \text{ GtC yr}^{-1}$). The methodology was required to produce a consistent climate-carbon cycle equilibrium state, without the computational expense of running the entire coupled model for thousands of simulated years.

Table 2 shows the multistage process used. The first two stages are primarily concerned with producing an equilibrium distribution of dissolved carbon in the ocean model (Jones and Palmer (1998)). In the first stage the ocean-atmosphere GCM was integrated forward for approximately 60 years, using a prescribed “pre-industrial” CO_2 concentration of 290 ppmv. The initial ocean physical state was based on temperature and salinity data from the Levitus climatology (Levitus and Boyer (1994), Levitus *et al* (1994)). During this stage the modelled sea surface temperature and salinity were relaxed to the climatology (i.e. “Haney forced”), with a relaxation timescale of about 2 weeks. This stage also included the TRIFFID dynamic global vegetation model used in “equilibrium” mode. Vegetation and soil variables were updated iteratively every 5 model years, using an implicit scheme with a long internal timestep (≈ 1000 years). This approach is equivalent to a Newton-Raphson algorithm for approaching equilibrium, and offline tests have shown that it is very effective in producing equilibrium states for the slowest variables (e.g. soil carbon and forest cover).

The second stage was a long run of approximately 2000 years in ocean-only mode using the distorted physics technique (Bryan (1984), Wood (1998)), which allows a lengthened timestep of 24 hours to be used. This enables a long period to be simulated quickly and cheaply, allowing the deep ocean structure to come close to equilibrium. Climatological temperature and salinity data were again used to Haney force the ocean-surface with the same coefficients as before. Other fluxes were derived from monthly mean values calculated from the last ten years of the coupled phase, with daily variability imposed from the last year of the run. The daily variability was found to be crucial in allowing realistic mixed layer depths to be maintained in the ocean only phase (Jones and Palmer (1998)). The forcing fluxes used were; penetrative solar heat flux, non-penetrative heat flux, wind mixing energy, wind stress (N-S and E-W components) and net fresh water flux (precipitation minus evaporation). The driving fluxes were modified to include the effects of sea-ice in the coupled phase, allowing the ocean-only phase to be carried out without an interactive sea-ice model.

In the third stage the ocean was recoupled to the atmosphere model, using the ocean state from the end of the ocean-only phase, but still Haney-forcing the ocean surface state back to the climatology. TRIFFID was switched to its default dynamic mode, in which the vegetation cover is updated every 10 days. A 90-year run was carried out to allow the coupled model to adjust to the introduction of short timescale vegetation variability, and to define heat and freshwater “flux-adjustments” for the subsequent stages.

Stage 4 saw the introduction of internally-generated SST variability for the first time, as the Haney forcing terms were switched-off and replaced by these fixed adjustments. This was the point when the

impact of El Nino events on the carbon balance became obvious (Jones *et al* (submitted)). A 60-year simulation was completed to give the system ample time to adjust.

Finally, the atmospheric CO₂ was treated as an interactive variable in stage 5. All previous stages had used a prescribed CO₂ concentration. A short fully-interactive climate-carbon cycle run (of about 20 years) was carried out to ensure that there were no significant drifts in the atmospheric CO₂ concentration. Results from the subsequent pre-industrial simulation of 100 years are discussed in the next section.

b The Mean Pre-Industrial State

b.1 The Ocean Carbon Cycle

HadOCC explicitly models the ocean ecosystem in order to represent the biological pump. The two main processes of this pump are primary production and the sinking flux of organic carbon and the HadOCC model has been shown to compare well to observations for both these processes (Palmer and Totterdell (in press)). The global annual total production in the model is about 53 GtC yr⁻¹, while recent satellite-derived estimates are 39.4 Antoine *et al* (1996), 48.5 and 49.4 Longhurst *et al* (1990) GtC yr⁻¹. Considering these estimates refer to net production (including respiration losses) and the model's figure is for gross production, the model is well within the range of observational estimates.

Figure 3 shows the zonal total of primary production for each month averaged over the 100 years of the control simulation. Also shown for comparison is the zonal total of primary production from the climatology of Antoine *et al* (1996). The seasonal cycle in primary production is captured by the ocean ecosystem model. The magnitude in the model is higher than suggested by Antoine *et al* (1996) but that study has the lowest total production of the three climatologies mentioned above. In the equatorial Pacific the model overestimates primary production. This is a result of excessive upwelling of nutrients at the equator, but also the model does not represent more complex limitations on production. These include, for example, iron limitation and ammonia inhibition, which have been suggested as important processes in High Nutrient Low Chlorophyll (HNLC) regions such as the equatorial Pacific (Loukas *et al* (1997)).

c The Land Carbon Cycle

The performance of the terrestrial component is best assessed by comparing its simulation of the global distribution of vegetation types to that observed. Figure 4 shows the fractional coverage of the 5 TRIFFID plant functional types and bare soil from the end of the pre-industrial control. The locations of the major forests and deserts are generally well captured. However, the boreal forests tend to be a little too sparse, especially in Siberia where the atmospheric model has a cold bias in winter. The absence of a cold-deciduous plant functional type in TRIFFID may also be a contributory factor here. If anything, the simulated tropical forests are too extensive, perhaps because of the neglect of various disturbance factors (e.g. fire and anthropogenic deforestation). This TRIFFID simulation includes some prescribed agricultural regions, in which grasslands are assumed to dominate (elsewhere forests dominate where they can survive). This ensures that the heavily cultivated mid-latitudes are simulated as grasslands. The competition between C₃ and C₄ grasses is simulated in the model, producing a dominance of C₄ in the semi-arid tropics and a dominance of C₃ elsewhere. However, this balance may be expected to shift as atmospheric CO₂ increases.

Panel g of figure 4 compares this simulation to the IGBP land-cover dataset derived from remote sensing. The fractional agreement in each gridbox, f_{agree} , is calculated as the maximum overlap between the vegetation fractions from the model (ν_i^{mod}) and the observations (ν_i^{obs}):

$$f_{agree} = 1 - \sum_{i=1}^5 |\nu_i^{mod} - \nu_i^{obs}| \quad (2)$$

where i labels the vegetation type. By this measure, TRIFFID reproduces 63% of the IGBP land-cover in this coupled simulation. The level of agreement is lower in the regions of north-east Eurasia which

are dominated by cold-deciduous spruce forests and in the savanna regions of Africa, but higher in the mid-latitudes and the tropical forests.

The simulated global totals for vegetation carbon (493 GtC) and soil carbon (1180 GtC) are consistent with other studies (Schimel *et al* (1996), Zinke *et al* (1986), Cramer *et al* (in press)). The integrated land net primary productivity (NPP) associated with this vegetation distribution is about 60 Gt C yr^{-1} , which is also within the range of other estimates (Warnant *et al* (1994), Cramer *et al* (in press)) and almost identical to the value suggested by Houghton *et al* (1996) for the present-day carbon cycle. Since the value simulated here corresponds to a “pre-industrial” CO_2 concentration of 290 ppmv, we expect slightly higher NPP to be simulated for the present-day.

d Interannual Variability

Figure 5 shows the annual mean CO_2 flux to the atmosphere over 100 years of the pre-industrial control simulation (lower panel), along with the contributions to this from the ocean and the terrestrial biosphere. The 20 year running mean of the total flux lies within the quality bounds of $\pm 0.4 \text{ GtC yr}^{-1}$ which we required for the equilibrium. It is also very clear that the modelled carbon cycle displays significant interannual variability about this equilibrium state. Variability in the total flux, and thus the atmospheric CO_2 concentration, is dominated by the contribution from the terrestrial biosphere. The net fluxes from the ocean and the land tend to have opposite signs, but the magnitude of the variability in the land fluxes is far larger.

This interannual variability in the modelled carbon cycle is found to be correlated with the El Nino Southern Oscillation (ENSO). This is illustrated by considering the Nino3 index. The Nino3 index is a measure of the ENSO cycle and is the sea surface temperature (SST) anomaly over the region 150°W - 90°W , 5°S - 5°N in the Equatorial Pacific. Under El Nino conditions, there is reduced ocean upwelling, less cooler water being brought to the surface, a positive SST anomaly and positive Nino3 index. Conversely La Nina conditions are characterised by greater upwelling, a negative SST anomaly and negative Nino3 index. When the Nino3 index is positive the model simulates an increase in atmospheric CO_2 resulting from the combined effect of the terrestrial biosphere acting as a large source, which is only partially offset by a reduced outgassing from the tropical Pacific. The opposite is true during the La Nina phase.

How realistic is this ENSO-driven variability in CO_2 ? In order to answer this question Jones *et al* (submitted) analysed the long-term records of atmospheric CO_2 concentration taken at Mauna Loa, Hawaii since 1958 (Keeling 1989). In these records, superimposed on the seasonal cycle and the long-term upward trend is interannual variability which cannot be readily explained by changes in fossil fuel burning. The correlation between these interannual changes in atmospheric CO_2 and the ENSO cycle was first reported in the 1970s (Bacastow 1976, Bacastow *et al* 1980). Figure 6 plots the anomaly in the growth rate of atmospheric CO_2 against the Nino3 index, from the pre-industrial control simulation and the Mauna Loa observations. In both cases the atmospheric CO_2 anomaly is positive during El Nino (positive Nino3) and decreases during La Nina (negative Nino3). The model appears to slightly overestimate the interannual variability in CO_2 because the amplitude of its internally-generated ENSO is too large.

The gradients of the blue dashed and red dashed lines represent the sensitivity of the carbon cycle to ENSO, as given by the model and the observations respectively. Here, we have excluded observations which immediately follow major volcanic events (black stars), since during these years the carbon cycle will also have been perturbed by the induced tropospheric cooling (Jones and Cox (in press)). These lines are almost parallel, suggesting that the modelled carbon cycle has a realistic sensitivity to ENSO. This is most important, since a realistic response to internally-generated climate anomalies is required before we can have any confidence in using the model to predict the response of the carbon cycle to anthropogenic forcing.

4 A First Transient Climate-Carbon Cycle Simulation

A transient coupled climate-carbon cycle simulation was carried out for 1860-2100, starting from the pre-industrial control state, and using CO₂ emissions as given by the IS92a scenario (Houghton *et al* (1992)). These emissions included a contribution from net land-use change (e.g. deforestation, forest regrowth), since TRIFFID does not yet model the effect of these interactively. The concentrations of the other major greenhouse gases were also prescribed from IS92a, but the radiative effects of sulphate aerosols were omitted in this first simulation.

Figure 7 shows the changing carbon budget in the fully coupled run (Cox *et al* (2000)). The continuous black line represents the simulated change in CO₂ since 1860 (in GtC), and the coloured lines show the contribution to this change arising from emissions (red), and changes in the carbon stored on the land (green) and in the oceans (blue). Net uptake by the land or the ocean since 1860, is represented by negative values, since this acts to reduce the change in atmospheric carbon. The gradients of these lines are equivalent to the annual mean fluxes in GtC yr⁻¹.

The dotted black line shows the change in atmospheric carbon given by the standard IS92a CO₂ *concentration* scenario, which has been often used to drive GCM climate predictions. This scenario was calculated with offline carbon cycle models which neglected the effects of climate change (Enting *et al* (1994)). A simulation with our coupled climate-carbon cycle model produced similar increases in CO₂ when the carbon cycle components were artificially isolated from the climate change. The difference between the continuous black line and the dashed black line therefore represents an estimate of the effect of climate-carbon cycle feedbacks on atmospheric CO₂.

a 1860-2000

From 1860 to 2000, the simulated stores of carbon in the ocean and on land increase by about 100 GtC and 75 GtC respectively (figure 7). The land uptake is largely due to CO₂-fertilisation of photosynthesis, which is partially counteracted by increasing respiration rates in the warming climate (Cramer *et al* (in press)). The ocean uptake is also driven by the increasing atmospheric CO₂, which results in a difference in the partial pressure of CO₂ across the ocean surface (equation 1). During this period, both components of the modelled carbon cycle are therefore producing a negative feedback on the CO₂ increase due to anthropogenic emissions.

However, the modelled atmospheric CO₂ is 15 to 20 ppmv too high by the present day, which corresponds to a timing error of about 10 years. Possible reasons for this include an overestimate of the prescribed net land-use emissions and the absence of other important climate forcing factors. The modelled global mean temperature increase from 1860 to 2000 is about 1.4 K (figure 10b), which is higher than observed (Nicholls *et al* (1996)). This may have led to an excessive enhancement of respiration fluxes over this period. The overestimate of the historical warming is believed to be due to the neglect of the cooling effects of anthropogenic aerosols (Mitchell *et al* (1995)).

We have recently completed a further coupled climate-carbon cycle experiment which includes the effects of aerosols from volcanoes, as well as those from human activity, along with the additional radiative forcing factor from solar variability. This experiment produces a much better fit to the observed increase in global mean temperature, halving the overestimate of current CO₂ to 5-10 ppmv. The remaining “error” is almost certainly within the bounds of uncertainties associated with the prescribed net land-use emissions.

Nevertheless, the coupled model does a good job of simulating the recent carbon balance. For the 20 years centred on 1985, the mean land and ocean uptake are 1.5 and 1.6 GtC yr⁻¹ respectively (c.f. best estimates for the 1980s of 1.8±1.8 and 2.0±0.8 GtC yr⁻¹ (Schimel *et al* (1996))).

b 2000-2100

The simulated atmospheric CO₂ diverges much more rapidly from the standard IS92a concentration scenario in the future. The ocean takes up about 400 GtC over this period, but at a rate which is asymptoting towards 5 GtC yr⁻¹ by 2100. This reduced efficiency of oceanic uptake is partly a

consequence of the non-linear dependence of the partial pressure of dissolved CO₂ (pCO₂) on total ocean carbon concentration (TCO₂), but may also have contributions from climate change (Sarmiento *et al* (1998)). Although the thermohaline circulation weakens by about 25% from 2000 to 2100, this is much less of a reduction than seen in some previous simulations (Sarmiento and Quere (1996)), and the corresponding impact on ocean carbon uptake is less significant. In this experiment, increased thermal stratification due to warming of the sea-surface suppresses upwelling, which reduces nutrient availability and lowers primary production by about 5%. However, ocean-only tests suggest a small climate-change impact on oceanic carbon uptake, since this reduction in the biological pump is compensated by reduced upwelling of deepwaters which are rich in TCO₂.

The most marked impacts of climate-carbon cycle feedbacks are seen in the terrestrial biosphere, which switches from being a weak sink to become a strong source of carbon from about 2050. (Note how the gradient of the green line in figure 7 becomes positive from this time.) There are two main reasons for this. Firstly, the GCM predicts an appreciable drying and warming in the Amazon basin, which results in “dieback” of the tropical rainforest and a release of carbon to the atmosphere. Similar CO₂-induced climate changes have been predicted by other GCMs for this region (Gedney *et al* (2000)), but the magnitude of these seems largest in the latest Hadley Centre models. This may be partly because the Hadley Centre models include CO₂-induced stomatal closure, which seems particularly to reduce evaporation and rainfall in Amazonia (Cox *et al* (1999)). A similar terrestrial response was also produced by a very different ecosystem model when driven offline by anomalies from HadCM3 (White *et al* (1999)). We might expect an even more dramatic change in HadCM3LC since for the first time the climate-induced dieback of the forest is able to produce further reductions in precipitation and increases in surface temperature, via biophysical feedbacks.

The second reason for the sink-to-source transition in the terrestrial biosphere is a widespread loss of soil carbon. Broadly speaking, a rise in CO₂ alone tends to increase the rate of photosynthesis and thus terrestrial carbon storage, providing other resources are not limiting (Melillo *et al* (1995), Cao and Woodward (1998)). However, plant maintenance and soil respiration rates both increase with temperature. As a consequence, climate warming (the indirect effect of a CO₂ increase) tends to reduce terrestrial carbon storage (Cramer *et al* (in press)), especially in the warmer regions where an increase in temperature is not beneficial for photosynthesis. At low CO₂ concentrations the direct effect of CO₂ dominates, and both vegetation and soil carbon increase with atmospheric CO₂. However, as CO₂ rises further, terrestrial carbon begins to decrease, since the direct effect of CO₂ on photosynthesis saturates but the specific soil respiration rate continues to increase with temperature. The transition between these 2 regimes occurs abruptly at around 2050 in this experiment.

Figure 8 shows how zonal mean soil and vegetation carbon change through the simulation. The model suggests that carbon accumulation in natural ecosystems to date has occurred in the soils and vegetation of the northern mid-latitudes, and in the vegetation of the tropics. In the simulation, carbon continues to be accumulated in the northern hemisphere vegetation, but at a reducing rate from about 2070 onwards. The loss of tropical biomass beginning in about 2030 is very clearly shown in figure 8a. The rapid reduction in soil carbon seems to start around 2050 in the tropics, and around 2070 in the mid-latitudes. Note however, that soil carbon continues to increase in the far north until the end of the run.

Figure 9 shows maps of the changes in vegetation and soil carbon from 1860 to 2100. The increase of biomass in the northern hemisphere can be seen to arise from a thickening of the boreal forests. The reduction in Amazonian vegetation is also obvious. Losses of soil carbon, relative to 1860, are more widespread with reductions in most areas south of 60°N. South-east Asia, and the tundra-covered areas of Siberia and Alaska, are amongst the few regions to have more soil carbon in 2100 than in 1860.

Overall, the land carbon storage decreases by about 170 GtC from 2000 to 2100, accelerating the rate of CO₂ increase in the next century. By 2100 the modelled CO₂ concentration is about 980 ppmv in the coupled experiment, which is more than 250 ppmv higher than the standard IS92a scenario (figure 10a). This difference is equivalent to about 500 GtC (rather than 170 GtC), because the standard scenario implicitly assumes a continuing terrestrial carbon sink, accumulating to about

As a result of these climate-carbon cycle feedbacks, global-mean and land-mean temperatures increase from 1860 to 2100 by about 5.5K and 8K respectively, rather than about 4K and 5.5K, under the standard concentration scenario (figure 10b).

5 Discussion

These numerical experiments demonstrate the potential importance of climate-carbon cycle feedbacks, but the magnitude of these in the real Earth system is still highly uncertain. The strongest feedbacks, and therefore the greatest uncertainties, seem to be associated with the terrestrial biosphere. The cause of the present day land carbon sink is still in doubt, with CO₂-fertilisation, nitrogen deposition and forest regrowth all implicated in certain regions. The location of this sink is even more debatable, perhaps because this is subject to great interannual variability. Whilst increases in atmospheric CO₂ are expected to enhance photosynthesis (and reduce transpiration), the associated climate warming is likely to increase plant and soil respiration. Thus there is a competition between the direct effect of CO₂, which tends to increase terrestrial carbon storage, and the indirect effect, which may reduce carbon storage.

The outcome of this competition has been seen in a range of DGVMs (Cramer *et al* (in press)), each of which simulate reduced land carbon under climate change alone and increased carbon storage with CO₂ increases only. In most DGVMs, the combined effect of the CO₂ and associated climate change results in a reducing sink towards the end of the 21st century, as CO₂-induced fertilisation begins to saturate but soil respiration continues to increase with temperature. The manner in which soil and plant respiration respond in the long-term to temperature is a key uncertainty in the projections of CO₂ in the 21st century (Giardina and Ryan (2000)).

a Sink-to-Source Transitions in the Terrestrial Carbon Cycle

In this sub-section we introduce a simple terrestrial carbon balance model to demonstrate how the conversion of a land CO₂ sink to a source is dependent on the responses of photosynthesis and respiration to CO₂ increases and climate warming. We consider the total carbon stored in vegetation and soil, C_T , which is increased by photosynthesis, Π , and reduced by the total ecosystem respiration, R :

$$\frac{dC_T}{dt} = \Pi - R \quad (3)$$

where Π is sometimes called Gross Primary Productivity (GPP), and R represents the sum of the respiration fluxes from the vegetation and the soil. In common with many others (McGuire *et al* (1992), Collatz *et al* (1991), Collatz *et al* (1992), Sellers *et al* (1996b), Cox *et al* (1998)), we assume that GPP depends directly on the atmospheric CO₂ concentration, C_a , and the surface temperature, T (in °C):

$$\Pi = \Pi_{max} \left\{ \frac{C_a}{C_a + C_{0.5}} \right\} f(T) \quad (4)$$

where Π_{max} is the value which GPP asymptotes towards as $C_a \rightarrow \infty$, $C_{0.5}$ is the “half-saturation” constant (i.e. the value of C_a for which Π is half this maximum value), and $f(T)$ is an arbitrary function of temperature. We also assume that the total ecosystem respiration, R , is proportional to the total terrestrial carbon, C_T . The specific respiration rate (i.e. the respiration per unit carbon) follows a “Q10” dependence, which means that it increases by a factor of q_{10} for a warming of T by 10°C. Thus the ecosystem respiration rate is given by:

$$R = r C_T q_{10}^{(T-10)/10} \quad (5)$$

where r is the specific respiration rate at $T = 10^\circ\text{C}$. It is more usual to assume separate values of r and q_{10} for different carbon pools (e.g. soil/vegetation, leaf/root/wood), but our simpler assumption

will still offer good guidance as long as the relative sizes of these pools do not alter significantly under climate change. Near surface temperatures are expected to increase approximately logarithmically with the atmospheric CO₂ concentration, C_a (Huntingford and Cox (2000)):

$$\Delta T = \frac{\Delta T_{2 \times CO_2}}{\log 2} \log \left\{ \frac{C_a}{C_a(0)} \right\} \quad (6)$$

where ΔT is the surface warming, $\Delta T_{2 \times CO_2}$ is the climate sensitivity to doubling atmospheric CO₂, and $C_a(0)$ is the initial CO₂ concentration. We can use this to eliminate CO₂ induced temperature changes from equation 5:

$$R = r_0 C_T \left\{ \frac{C_a}{C_a(0)} \right\}^\alpha \quad (7)$$

where $r_0 C_T$ is the initial ecosystem respiration (i.e. at $C_a = C_a(0)$) and the exponent α is given by:

$$\alpha = \frac{\Delta T_{2 \times CO_2}}{10} \frac{\log q_{10}}{\log 2} \quad (8)$$

We can now use equations 3, 4 and 7 to solve for the equilibrium value of terrestrial carbon, C_T^{eq} :

$$C_T^{eq} = \Pi_{max} \left\{ \frac{C_a}{C_a + C_{0.5}} \right\} \left\{ \frac{C_a(0)}{C_a} \right\}^\alpha \frac{f(T)}{r_0} \quad (9)$$

The land will tend to amplify CO₂-induced climate change if C_T^{eq} decreases with increasing atmospheric CO₂ (i.e. $dC_T^{eq}/dC_a < 0$). Differentiating equation 9 with respect to C_a yields:

$$\frac{dC_T^{eq}}{dC_a} = C_T^{eq} \left[\frac{(1 - \alpha_*)}{C_a} - \frac{1}{C_a + C_{0.5}} \right] \quad (10)$$

where:

$$\alpha_* = \frac{\Delta T_{2 \times CO_2}}{\log 2} \left\{ \frac{\log q_{10}}{10} - \frac{1}{f} \frac{df}{dT} \right\}. \quad (11)$$

The condition for the land to become a source of carbon under increasing CO₂ is therefore:

$$C_a > \frac{1 - \alpha_*}{\alpha_*} C_{0.5} \quad (12)$$

This means that there will always be a critical CO₂ concentration beyond which the land becomes a source, as long as:

- (i) CO₂ fertilisation of photosynthesis saturates at high CO₂, i.e. $C_{0.5}$ is finite.
- (ii) $\alpha_* > 0$, which requires:
 - (a) climate warms with increasing CO₂, i.e. $\Delta T_{2 \times CO_2} > 0$
 - (b) respiration increases more rapidly with temperature than GPP, i.e.

$$\frac{\log q_{10}}{10} > \frac{1}{f} \frac{df}{dT}. \quad (13)$$

Conditions (i) and (ii)(a) are satisfied in the vast majority of climate and terrestrial ecosystem models. Detailed models of leaf photosynthesis indicate that $C_{0.5}$ will vary with temperature from about 300 ppmv at low temperatures, up to about 700 ppmv at high temperatures (Collatz *et al* (1991)). Although there are differences in the magnitude and patterns of predicted climate change, all GCMs produce a warming when CO₂ concentration is doubled. The global mean climate sensitivity produced by these models ranges from 1.5K to 4.5K (Houghton *et al* (1996)), but mean warming over land is

likely to be a more appropriate measure of the climate change experienced by the land biosphere. We estimate a larger range of $2\text{K} < \Delta T_{2\times\text{CO}_2} < 7\text{K}$, because the land tends to warm more rapidly than the ocean (Huntingford and Cox (2000)).

There is considerable disagreement over the likely long-term sensitivity of respiration fluxes to temperature, with some suggesting that temperature-sensitive “labile” carbon pools will soon become exhausted once the ecosystem enters a negative carbon balance (Giardina and Ryan (2000)). However, condition (ii)(b) is satisfied by the vast majority of existing land carbon cycle models, and seems to be implied (at least on the 1-5 year timescale) by climate-driven interannual variability in the measured atmospheric CO_2 concentration (Jones and Cox (in press), Jones *et al* (submitted)).

Most would therefore agree that the terrestrial carbon sink has a finite lifetime, but the length of this lifetime is highly uncertain. We can see why this is from our simple model (equation 12). The critical CO_2 concentration is very sensitive to α_* which is itself dependent on the climate sensitivity, and the difference between the temperature dependences of respiration and GPP (equation 11).

We expect the temperature sensitivity of GPP to vary regionally, since generally a warming is beneficial for photosynthesis in mid and high latitudes (i.e. $df/dT > 0$), but not in the tropics where the existing temperatures are near optimal for vegetation (i.e. $df/dT \leq 0$). As a result, we might expect global mean GPP to be only weakly dependent on temperature ($df/dT \approx 0$). We can therefore derive a range for α_* , based on plausible values of climate sensitivity over land ($2\text{K} < \Delta T_{2\times\text{CO}_2} < 7\text{K}$) and respiration sensitivity ($1.5 < q_{10} < 2.5$). This range of $0.1 < \alpha_* < 0.9$, translates into a critical CO_2 concentration which is somewhere between 0.1 and 9 times the half-saturation constant (equation 12). Therefore on the basis of this simple analysis the range of possible critical CO_2 values spans almost 2 orders of magnitude. Evidently, the time at which the sink-to-source transition will occur is extremely sensitive to these uncertain parameters. This may explain why many of the existing terrestrial models do not reach this critical point before 2100 (Cramer *et al* (in press)).

Fortunately we can reduce the uncertainty range further. Critical CO_2 values which are lower than the current atmospheric concentration are not consistent with the observations, since the “natural” land ecosystems appear to be a net carbon sink rather than a source at this time (Schimel *et al* (1996)). For a typical half-saturation constant of $C_{0.5} = 500$ ppmv this implies that all combinations of q_{10} and $\Delta T_{2\times\text{CO}_2}$ which yield values of $\alpha_* < 0.6$ are unrealistic. Also, sensitivity tests with our coupled model indicate that $q_{10} = 2$ provides an almost optimal fit to the observed variability in atmospheric CO_2 due to ENSO (Jones *et al* (submitted)) and volcanic eruptions (Jones and Cox (in press)), suggesting that the probability distribution for possible q_{10} values is peaked quite sharply about this value. Similarly the complete range of climate sensitivity values are not all equally probable, since the most advanced GCMs tend to produce values clustered around the centre of the range. It is therefore meaningful to produce a central estimate for the critical CO_2 value. Using $q_{10} = 2$, $C_{0.5} = 500$ ppmv, and $\Delta T_{2\times\text{CO}_2} = 4.8\text{K}$ (which is consistent with the warming over land in our coupled model,) yields a critical CO_2 value of about 550 ppmv, which is remarkably close to the sink-to-source transition seen in our experiment (see figures 7 and 10a).

We draw two main conclusions from this section. The recognised uncertainties in climate and respiration sensitivity imply a very large range in the critical CO_2 concentration beyond which the land will act as a net carbon source. However, the central estimates for these parameters suggest a significant probability of this critical point being passed by 2100 in the real Earth system, under a “business as usual” emissions scenario, in agreement with the results from our coupled climate-carbon cycle model.

6 Conclusions

The ocean and the land ecosystems are currently absorbing about half the human emissions of CO_2 , but many of the uptake processes are known to be sensitive to climate. GCM climate change predictions typically exclude interactions between climate and the natural biosphere, since they use fixed vegetation distributions and CO_2 concentrations which are calculated offline neglecting climate change. We have developed a 3D coupled climate-carbon cycle model (“HadCM3LC”), by coupling models of

the ocean carbon cycle (“HadOCC”) and the terrestrial carbon cycle (“TRIFFID”) to a version of the Hadley Centre GCM. The methodology developed to spin-up the model has been shown to yield a pre-industrial equilibrium to good accuracy. The climate-carbon cycle model is able to reproduce key aspects of the observations, including the global distribution of vegetation types, seasonal and zonal variations in ocean primary production, and the interannual variability in atmospheric CO₂.

A transient simulation has been carried out with this model for 1860-2100 using the IS92a (“business as usual”) CO₂ emissions scenario. This experiment suggests that carbon cycle feedbacks could significantly accelerate atmospheric CO₂ rise and climate change over the next 100 years. The modelled terrestrial biosphere switches from being an overall sink for CO₂ to become a strong source from about 2050, as soil carbon starts to decline sharply and local climate change leads to significant loss of the Amazon rainforest. By 2100 the modelled CO₂ is more than 250 ppmv higher than that usually assumed in GCM climate-change experiments. The corresponding global-mean warming for 1860-2100 is about 5.5 K, as compared to 4 K without carbon cycle feedbacks.

The quantitative aspects of this experiment must be treated with caution, owing to uncertainties in the components of the coupled model. In particular, climate models differ in their responses to greenhouse gases, and terrestrial carbon models differ in their responses to climate change (VEMAP-Members (1995) Cramer *et al* (in press)). However, we have presented a simple analysis to demonstrate that a sink-to-source transition of the terrestrial biosphere is assured beyond some critical atmospheric CO₂ concentration, provided that a few simple conditions apply. Qualitatively then, the eventual saturation of the land carbon sink and its conversion to a carbon source, is supported by our existing understanding of terrestrial ecosystem processes.

Unfortunately, the precise point at which the land biosphere will start to provide a positive feedback cannot yet be predicted with certainty. This depends on a number of poorly understood processes, such as the long-term response of photosynthesis and soil respiration to increased temperatures (Giardina and Ryan (2000)), and the possible acclimation of photosynthesis to high CO₂. Our results suggest that accurate prediction of climate change over the 21st century, will be as dependent on advances in the understanding and modelling of these physiological and ecological processes, as it is on the modelling of the physical processes currently represented in GCMs.

Acknowledgements

This work was supported by the UK Department of the Environment, Transport and the Regions, under contract PECD 7/12/37.

References

- Antoine, D., J.-M. Andre, and A. Morel, 1996: Oceanic primary production 2. Estimation at global scale from satellite (Coastal Zone Color Scanner) chlorophyll. *Global Biogeochemical Cycles*, **10**, 57–69.
- Bacastow, R., and C. Keeling, 1981: Atmospheric CO₂ and the southern oscillation: effects associated with recent El Nino events. *WMO/ICSU/UNEP Scientific Conference on analysis and interpretation of atmospheric CO₂ data*, volume WCP 14 of *World Climate Programme*, WMO, World Clim. Prog. Off., Geneva.
- Berner, R., 1997: The rise of plants and their effect on weathering and atmospheric CO₂. *Nature*, **276**, 544–546.
- Betts, R. A., P. M. Cox, S. E. Lee, and F. I. Woodward, 1997: Contrasting physiological and structural vegetation feedbacks in climate change simulations. *Nature*, **387**, 796–799.
- Bryan, K., 1984: Accelerating the convergence to equilibrium of ocean–climate models. *Journal of Physical Oceanography*, **14**, 666–673.
- Cao, M., and F. I. Woodward, 1998: Dynamic responses of terrestrial ecosystem carbon cycling to global climate change. *Nature*, **393**, 249–252.

- Claussen, M., 1996: Variability of global biome patterns as a function of initial and boundary conditions in a climate model. *Climate Dynamics*, **12**, 371–379.
- Collatz, G. J., J. T. Ball, C. Grivet, and J. A. Berry, 1991: Physiological and environmental regulation of stomatal conductance, photosynthesis and transpiration: A model that includes a laminar boundary layer. *Agric. and Forest Meteorol.*, **54**, 107–136.
- , M. Ribas-Carbo, and J. A. Berry, 1992: A coupled photosynthesis-stomatal conductance model for leaves of C₄ plants. *Aus. J. Plant Physiol.*, **19**, 519–538.
- Cox, P. M., C. Huntingford, and R. J. Harding, 1998: A canopy conductance and photosynthesis model for use in a GCM land surface scheme. *J. Hydrology*, **212-213**, 79–94.
- , R. A. Betts, C. B. Bunton, R. L. H. Essery, P. R. Rowntree, and J. Smith, 1999: The impact of new land surface physics on the GCM simulation of climate and climate sensitivity. *Clim. Dyn.*, **15**, 183–203.
- Cox, P., R. Betts, C. Jones, S. Spall, and I. Totterdell, 2000: Acceleration of global warming due to carbon-cycle feedbacks in a coupled climate model. *Nature*, **408**, 184–187.
- Cramer, W., A. Bondeau, F. Woodward, I. Prentice, R. Betts, V. Brovkin, P. Cox, V. Fisher, J. Foley, A. Friend, C. Kucharik, M. Lomas, N. Ramankutty, S. Storch, B. Smith, A. White, and C. Young-Molling, in press: Global response of terrestrial ecosystem structure and function to CO₂ and climate change: Results from six dynamic global vegetation models. *Global Change Biol.*
- DOE, 1994: *Handbook of methods for the analysis of the various parameters of the carbon dioxide system in sea water; version 2*. U.S. DOE.
- Edwards, J. M., and A. Slingo, 1996: Studies with a flexible new radiation code. I: Choosing a configuration for a large-scale model. *Quart. J. Roy. Meteor. Soc.*, **122**, 689–720.
- Enting, I., T. Wigley, and M. Heimann, 1994: Future emissions and concentrations of carbon dioxide; key ocean/atmosphere/land analyses. Division of Atmospheric Research Technical Paper 31, CSIRO.
- Field, C., R. Jackson, and H. Mooney, 1995: Stomatal responses to increased CO₂: implications from the plant to the global scale. *Plant, Cell and Environment*, **18**, 1214–1225.
- Foley, J. A. et al., 1996: An integrated biosphere model of land surface processes, terrestrial carbon balance and vegetation dynamics. *Global Biogeochemical Cycles*, **10**(4), 603–628.
- Friend, A. D., H. H. Shugart, and S. W. Running, 1993: A physiology-based model of forest dynamics. *Ecology*, **74**, 797–797.
- Gedney, N., P. Cox, H. Douville, J. Polcher, and P. Valdes, 2000: Characterizing GCM land-surface schemes to understand their responses to climate change. *J. Clim.*, **13**, 3066–3079.
- Gent, P. R., and J. C. McWilliams, 1990: Isopycnal mixing in ocean circulation models. *J. Phys. Oceanogr.*, **20**, 150–155.
- Giardina, C., and M. Ryan, 2000: Evidence that decomposition rates of organic carbon in mineral soil do not vary with temperature. *Nature*, **404**, 858–861.
- Gordon, C., C. Cooper, C. A. Senior, H. Banks, J. M. Gregory, T. C. Johns, J. F. B. Mitchell, and R. A. Wood, 2000: The simulation of SST, sea ice extents and ocean heat transports in a version of the Hadley Centre coupled model without flux adjustments. *Clim. Dyn.*, **16**, 147–168.

- Houghton, J. T., B. A. Callander, and S. K. Varney, 1992: *Climate change 1992. The supplementary report to the IPCC scientific assessment*. Cambridge University Press, 200pp.
- , L. G. Meira Filho, B. A. Callander, N. Harris, A. Kattenberg, and K. Maskell, 1996: *Climate Change 1995 — The Science of Climate Change*. Cambridge University Press. 572 pp.
- Huntingford, C., and P. Cox, 2000: An analogue model to derive additional climate change scenarios from existing GCM simulations. *Clim. Dyn.*, **16**, 575–586.
- Johns, T. C., R. E. Carnell, J. F. Crossley, J. M. Gregory, J. F. B. Mitchell, C. A. Senior, S. F. B. Tett, and R. A. Wood, 1997: The second Hadley Centre coupled ocean-atmosphere GCM: Model description, spinup and validation. *Climate Dyn.*, **13**, 103–134.
- Jones, C., and P. Cox, in press: Modelling the volcanic signal in the atmospheric CO₂ record. *Global Biogeochem. Cycles*.
- Jones, C. D., and J. R. Palmer, 1998: Spin-up methods for HadCM3L. Climate Research Technical Note 84, Hadley Centre for Climate Prediction and Research.
- Jones, C., M. Collins, P. Cox, and S. Spall, submitted: The carbon cycle response to ENSO: A coupled climate–Carbon cycle model study. *J. Clim.*
- Kershaw, R., and D. Gregory, 1997: Parametrization of momentum transport by convection. Part I. Theory and cloud modelling results. *Quarterly Journal of the Royal Meteorological Society*, **123**(541), 1133–1151.
- Levitus, S., and T. P. Boyer, 1994: *World Ocean Atlas 1994, Volume 4: Temperature*. NOAA/NESDIS E/OC21. US Department of Commerce. 117pp.
- , R. Burgett, and T. P. Boyer, 1994: *World Ocean Atlas 1994, Volume 3: Salinity*. NOAA/NESDIS E/OC21. US Department of Commerce. 99pp.
- Longhurst, A., S. Sathyendranath, T. Platt, and C. Caverhill, 1990: An estimate of global primary production in the ocean from satellite radiometer data. *Journal of Plankton Research*, **17**, 1245–1271.
- Loukas, H., B. Frost, D. E. Harrison, and J. W. Murray, 1997: An ecosystem model with iron limitation of primary production in the equatorial Pacific at 140W. *Deep-Sea Research II*, **44**, 2221–2249.
- Lovelock, J., and L. Kump, 1994: The failure of climate regulation in a geophysiological model. *Nature*, **369**, 732–734.
- McGuire, A., J. Melillo, L. Joyce, D. Kicklighter, A. Grace, B. M. III, and C. Vorosmarty, 1992: Interactions between carbon and nitrogen dynamics in estimating net primary productivity for potential vegetation in North America. *Global Biogeochem. Cycles*, **6**, 101–124.
- Melillo, J. M., I. C. Prentice, G. D. Farquhar, E. D. Schulze, and O. E. Sala, 1995: Terrestrial biotic responses to environmental change and feedbacks to climate. *Climate Change 1995*, Houghton, J. T., L. G. M. Filho, B. A. Callander, N. Harris, A. Kattenberg, and K. Maskell, Eds., Cambridge University Press.
- Mitchell, J. F. B., T. C. Johns, J. M. Gregory, and S. F. B. Tett, 1995: Climate response to increasing levels of greenhouse gases and sulphate aerosols. *Nature*, **376**, 501–504.
- Nicholls, N., G. Gruza, J. Jouzel, T. Karl, L. Ogallo, and D. Parker, 1996: *Climate Change 1995. The Science of Climate Change.*, chapter 3. Observed Climate Variability and Change. Cambridge University Press.
- Palmer, J. R., and I. J. Totterdell, in press: Production and export in a global ocean ecosystem model. *Deep-Sea Res.*

- Peng, T.-H., 1987: Seasonal variability of carbon dioxide, nutrients and oxygen in the northern North Atlantic surface water: observations and a model. *Tellus*, **39B**, 439–458.
- Pope, V. D., M. L. Gallani, P. R. Rowntree, and R. A. Stratton, 2000: The impact of new physical parametrizations in the Hadley Centre climate model – HadAM3. *Climate Dyn.*, **16**, 123–146.
- Post, W. M., and J. Pastor, 1996: LINKAGES - an individual-based forest ecosystem model. *Climatic Change*, **34**, 253–261.
- Prentice, I., W. Cramer, S. P. Harrison, R. Leemans, R. A. Monserud, and A. M. Solomon, 1992: A global biome model based on plant physiology and dominance, soil properties and climate. *Journal of Biogeography*, **19**, 117–134.
- Raich, J., and W. Schlesinger, 1992: The global carbon dioxide flux in soil respiration and its relationship to vegetation and climate. *Tellus*, **44B**, 81–99.
- Sarmiento, J., and C. L. Quere, 1996: Oceanic carbon dioxide uptake in a model of century-scale global warming. *Nature*, **274**(5291), 1346–1350.
- , T. Hughes, R. Stouffer, and S. Manabe, 1998: Simulated response of the ocean carbon cycle to anthropogenic climate warming. *Nature*, **393**(6682), 245–249.
- Schimel, D., D. Alves, I. Enting, M. Heimann, F. Joos, D. Raynaud, T. Wigley, M. Prather, R. Derwent, D. Enhalt, P. Fraser, E. Sanhueza, X. Zhou, P. Jonas, R. Charlson, H. Rodhe, S. Sadasivan, K. P. Shine, Y. Fouquart, V. Ramaswamy, S. Solomon, J. Srinivasan, D. Albritton, R. Derwent, I. Isaksen, M. Lal, and D. Wuebbles, 1996: Radiative forcing of climate change. *Climate Change 1995. The Science of Climate Change*, Houghton, J. T., L. G. M. Filho, B. A. Callander, N. Harris, A. Kattenberg, and K. Maskell, Eds., Cambridge University Press, 65–131.
- Sellers, P. J., L. Bounoua, G. J. Collatz, D. A. Randall, D. A. Dazlich, S. O. Los, J. A. Berry, I. Fung, C. J. Tucker, C. B. Field, and T. G. Jensen, 1996a: Comparison of radiative and physiological effects of doubled atmospheric CO₂ on climate. *Science*, **271**, 1402–1406.
- Sellers, P., D. Randall, C. Collatz, J. Berry, C. Field, D. Dazlich, C. Zhang, and G. Collelo, 1996b: A revised land surface parameterisation (SiB2) for atmospheric GCMs. Part I: Model formulation. *Journal of Climate*, **9**, 676–705.
- Siegenthaler, U., and J. L. Sarmiento, 1993: Atmospheric carbon dioxide and the ocean. *Nature*, **365**, 119–125.
- Taylor, N., 1995: Seasonal uptake of anthropogenic CO₂ in an ocean circulation model. *Tellus. B*, **47**, 145–169.
- VEMAP-Members, 1995: Vegetation/ecosystem modelling and analysis project: comparing biogeography and biogeochemistry models in a continental-scale study of terrestrial responses to climate change and CO₂ doubling. *Global Biogeochemical Cycles*, **9**, 407–437.
- Wanninkhof, R., 1992: Relationship between wind speed and gas exchange over the ocean. *J. Geophys. Res.*, **97**, 7373–7382.
- Warnant, P., L. Francois, D. Strivay, and J.-C. Gerard, 1994: CARAIB: A global model of terrestrial biological productivity. *Global Biogeochemical Cycles*, **8**(3), 255–270.
- White, A., M. Cannell, and A. Friend, 1999: Climate change impacts on ecosystems and on the terrestrial carbon sink: a new assessment. *Global Environ. Change*, **9**.
- Wood, R. A., 1998: Timestep sensitivity and accelerated spinup of an ocean GCM with a complex mixing scheme. *J. Atmos. Ocean. Technol.*, **15**, 482–495.

- Woodward, F. I., T. M. Smith, and W. R. Emanuel, 1995: A global land primary productivity and phytogeography model. *Global Biogeochemical Cycles*, **9**, 471–490.
- Zinke, P. J., A. G. Stangenberger, W. M. Post, W. R. Emanuel, and J. S. Olson, 1986: Worldwide organic soil carbon and nitrogen data. NDP-018, Carbon Dioxide Information Center, Oak Ridge National Laboratory, Oak Ridge, Tennessee, USA.

Process	Feedback Mechanism	Timescale
Stomatal Response	Surface Energy Partitioning	minutes
Leaf Seasonality	Surface Characteristics	months-seasons
DMS from Plankton	Cloud Albedo	months-years
Vegetation Distribution	Surface Characteristics	1-10 ³ years
Land Carbon Storage	Atmospheric CO ₂	1-10 ³ years
Ocean Carbon Storage	Atmospheric CO ₂	10-10 ⁴ years
Enhanced Rock Weathering	Atmospheric CO ₂	>10 ⁵ years

Table 1: Biospheric feedbacks on weather and climate

Physical Model		Biology		Atmos.	Model
Mode	Ocean Forcing	HadOCC	TRIFFID	CO ₂	years
Coupled	Haney forced	no	equil.	fixed	~60
Ocean-only	Haney forced	yes	no	fixed	~2000
Coupled	Haney forced	yes	dynamic	fixed	~90
Coupled	flux-adjusted	yes	dynamic	fixed	~60
Coupled	flux-adjusted	yes	dynamic	Interactive	~20

Table 2: The stages used to spin-up the coupled model to its pre-industrial equilibrium.

Coupled Climate-Carbon Cycle Model

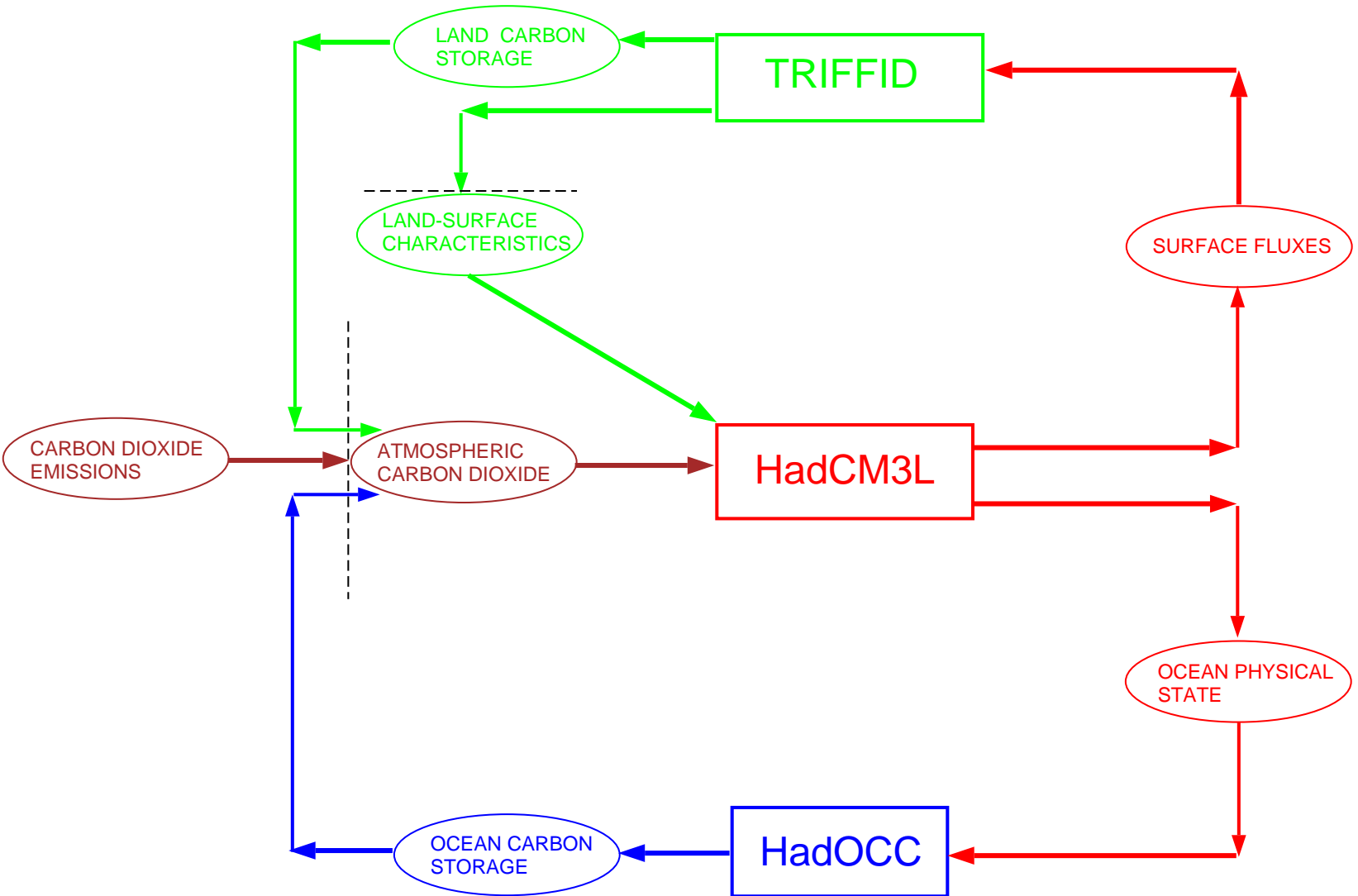


Figure 1: Schematic showing the structure of the coupled climate-carbon cycle model, which consists of the HadCM3L ocean-atmosphere GCM, the Hadley Centre Ocean Carbon Cycle model (HadOCC) and the TRIFFID dynamic global vegetation model. The coupled model enables two feedback loops to be closed; one associated with climate driven changes in atmospheric CO₂, and the other with biophysical feedbacks resulting from changes in the structure and distribution of vegetation. The dotted black lines denote where the loops are typically broken in standard GCM experiments.

TRIFFID Structure for a Single Plant Functional Type

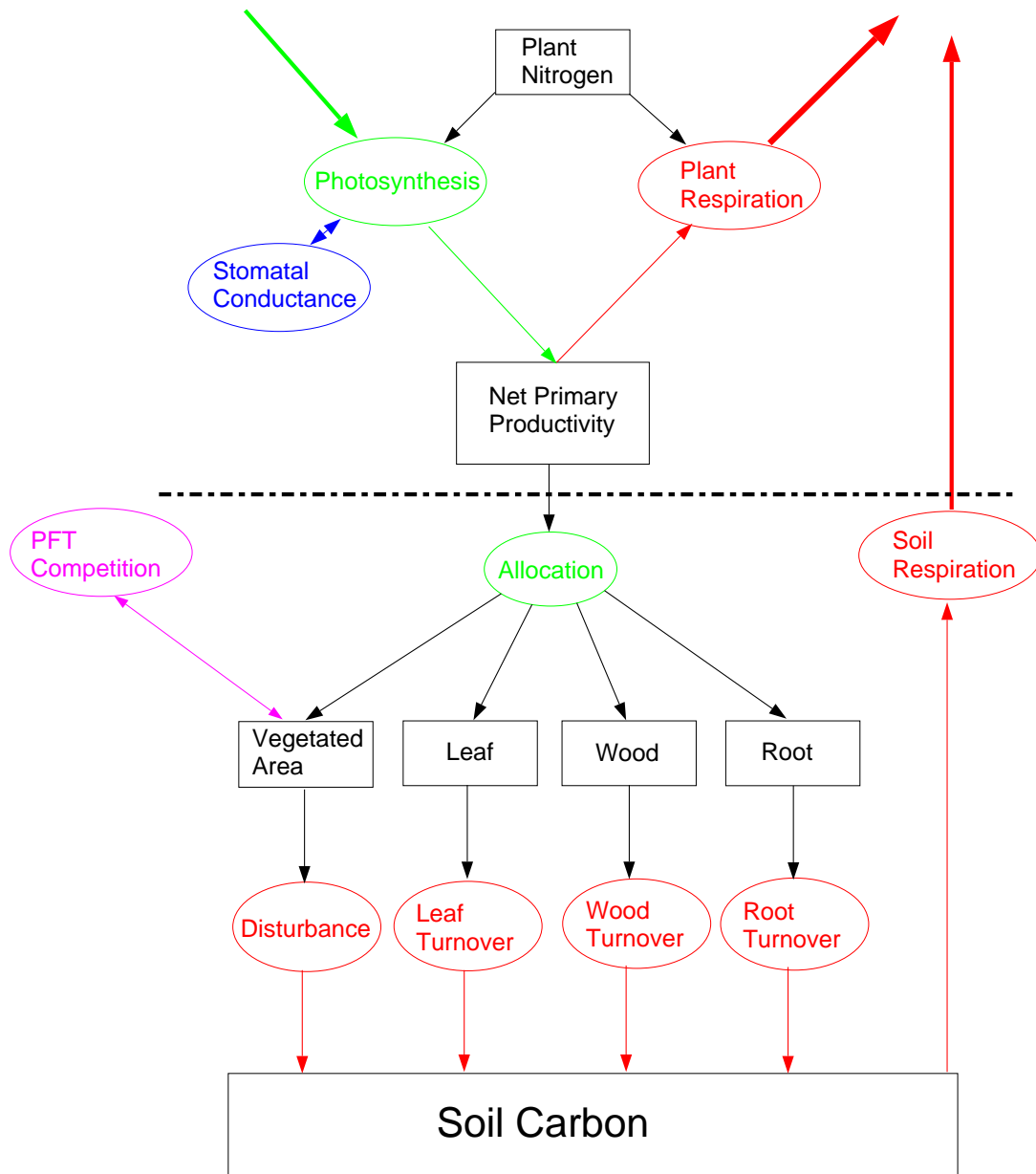


Figure 2: Schematic showing TRIFFID carbon flows for each vegetation type. Processes above the dotted line are fluxes calculated in the MOSES 2 land surface scheme every atmospheric model timestep (≈ 30 minutes). In dynamic mode, TRIFFID updates the vegetation and soil carbon every 10 days using time-averages of these fluxes.

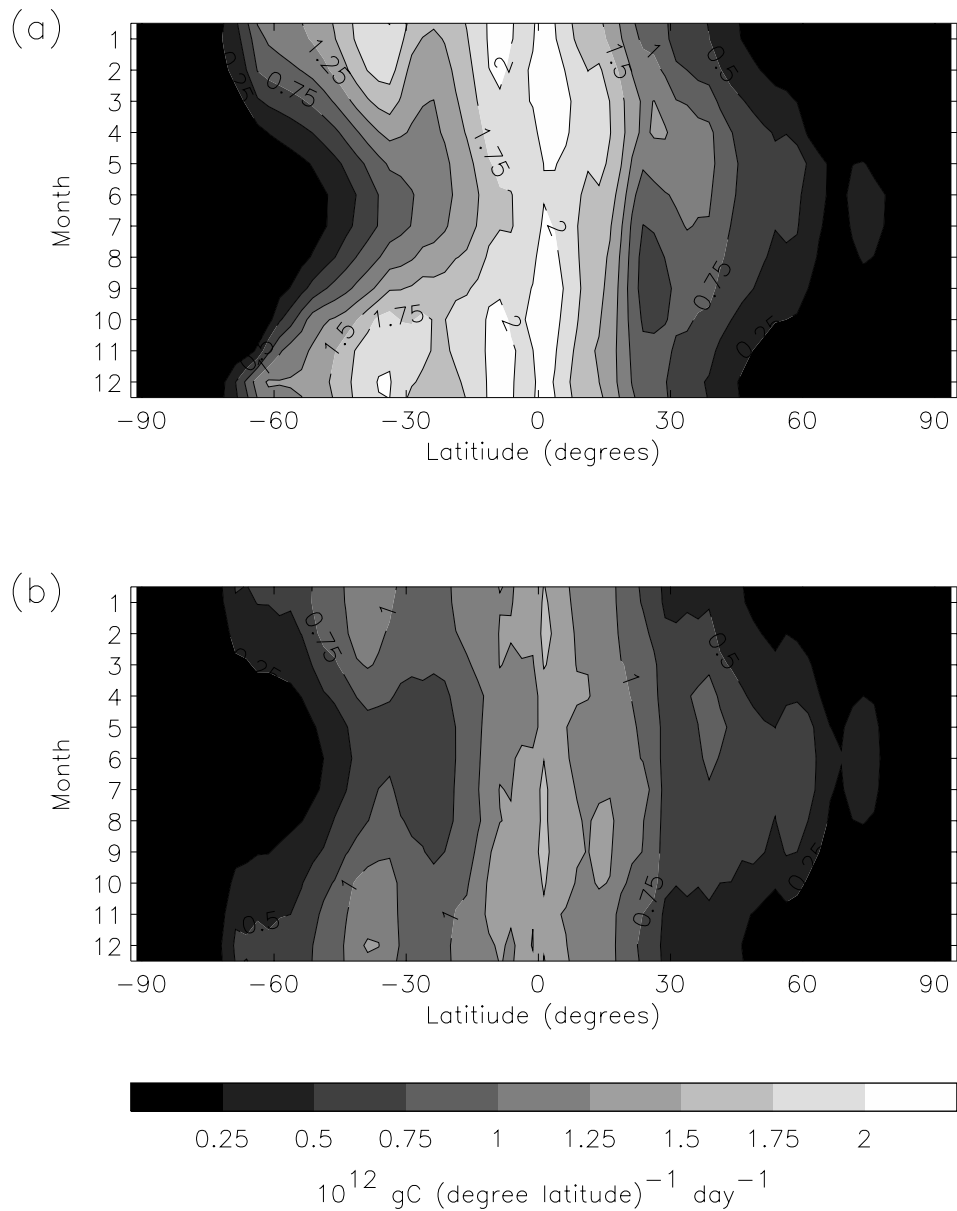


Figure 3: Ocean primary production as a function of latitude and month of the year. (a) Mean over 100 years of the control period. (b) The Antoine *et al.* (1996) satellite-derived climatology.

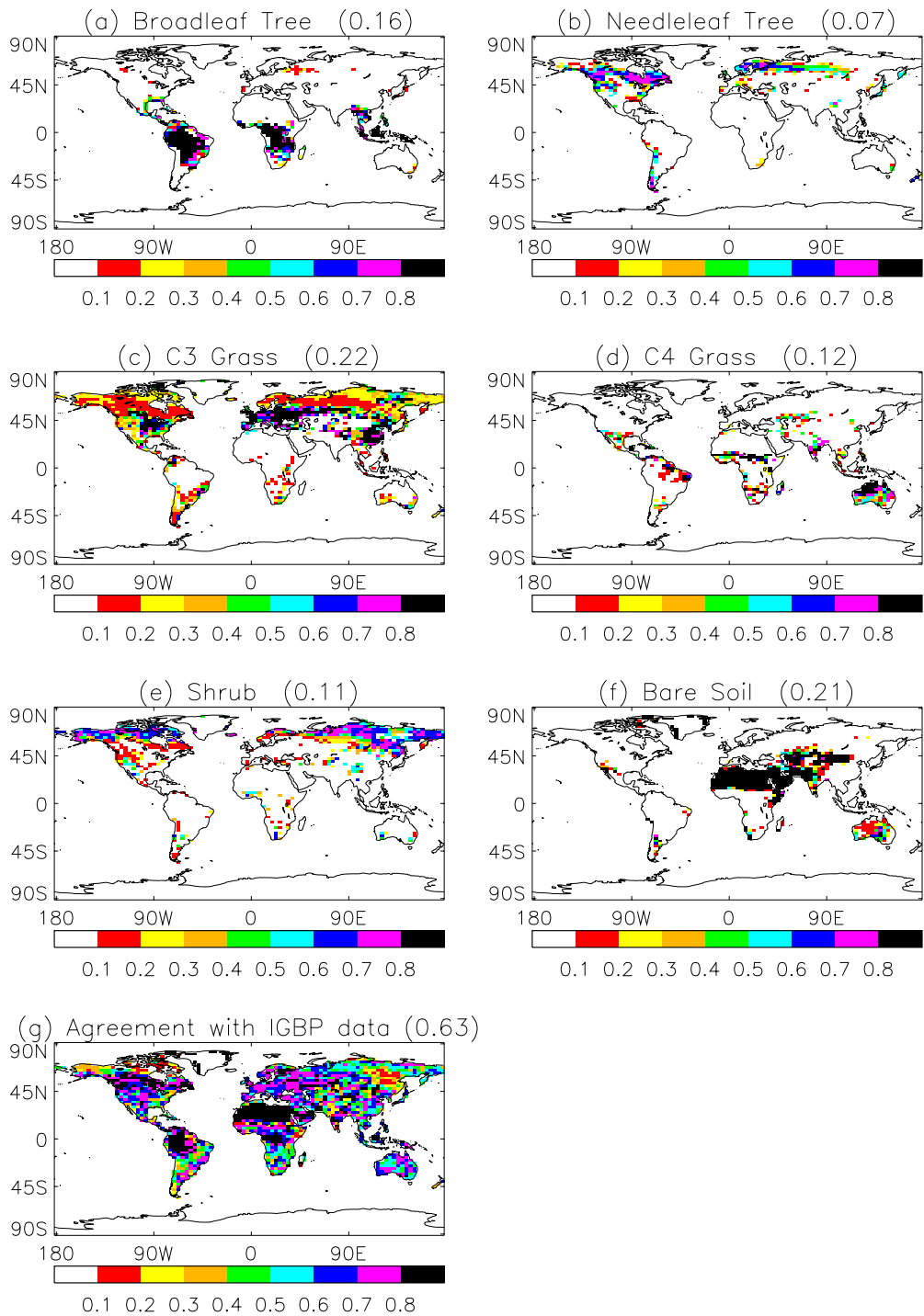


Figure 4: Annual mean fractional coverage of vegetation types ((a)-(e)) and bare soil (f) from 100 years of the pre-industrial control simulation. Plot (g) compares this simulation with the fractions of broadleaf tree, needleleaf tree, grass ($C_3 + C_4$) and shrub from the IGBP land-cover dataset. The numbers in brackets are means over the entire land area.

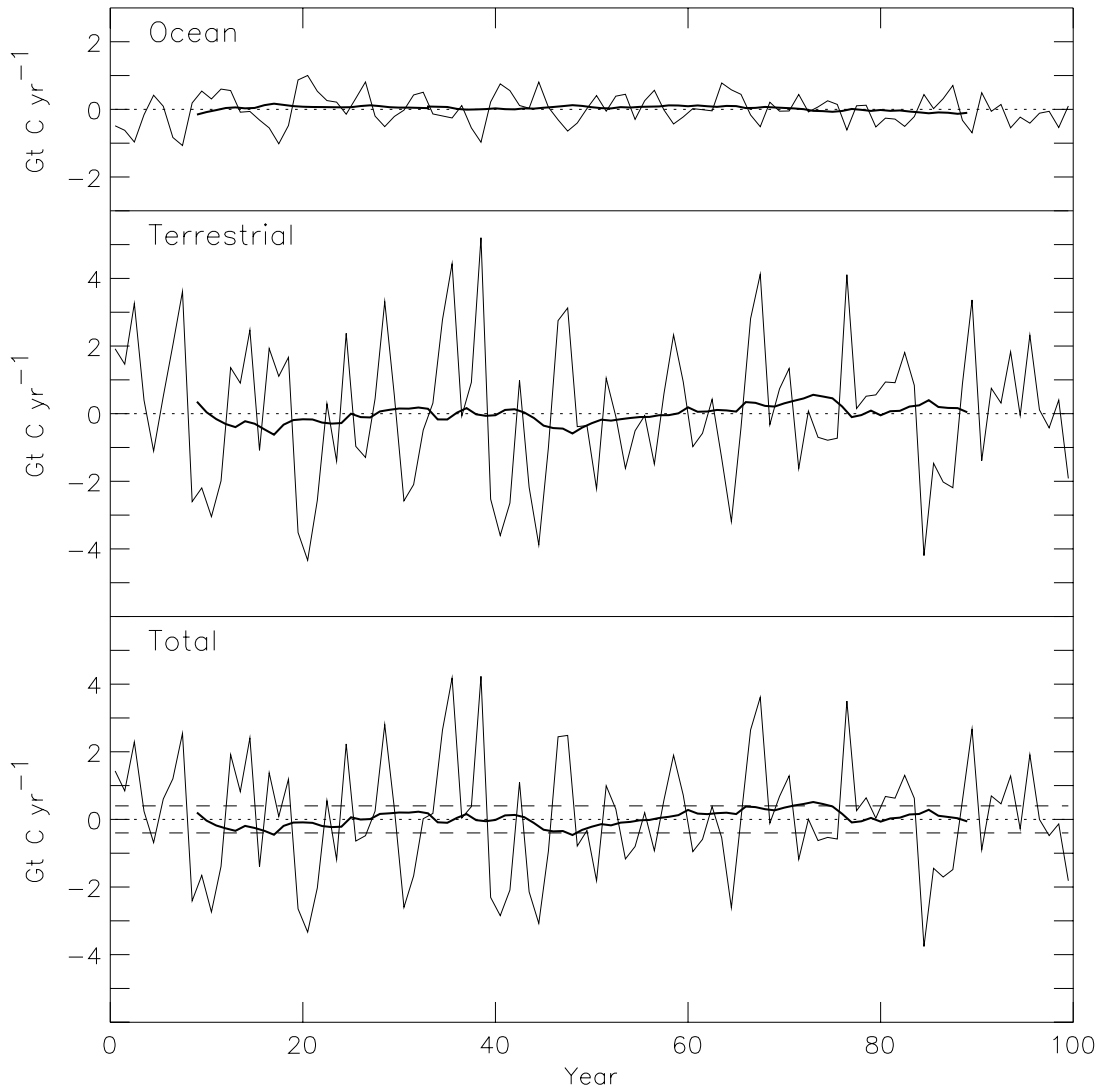


Figure 5: The total flux of CO₂ to the atmosphere as a function of year during the control period, along with contributions to this from the ocean and the terrestrial biosphere. The thin lines show the annual mean data and the thick lines are the 20 year running means of the annual data. In the plot for total flux, the dashed lines indicate the quality criterion required for the pre-industrial equilibrium of ± 0.4 GtC yr⁻¹.

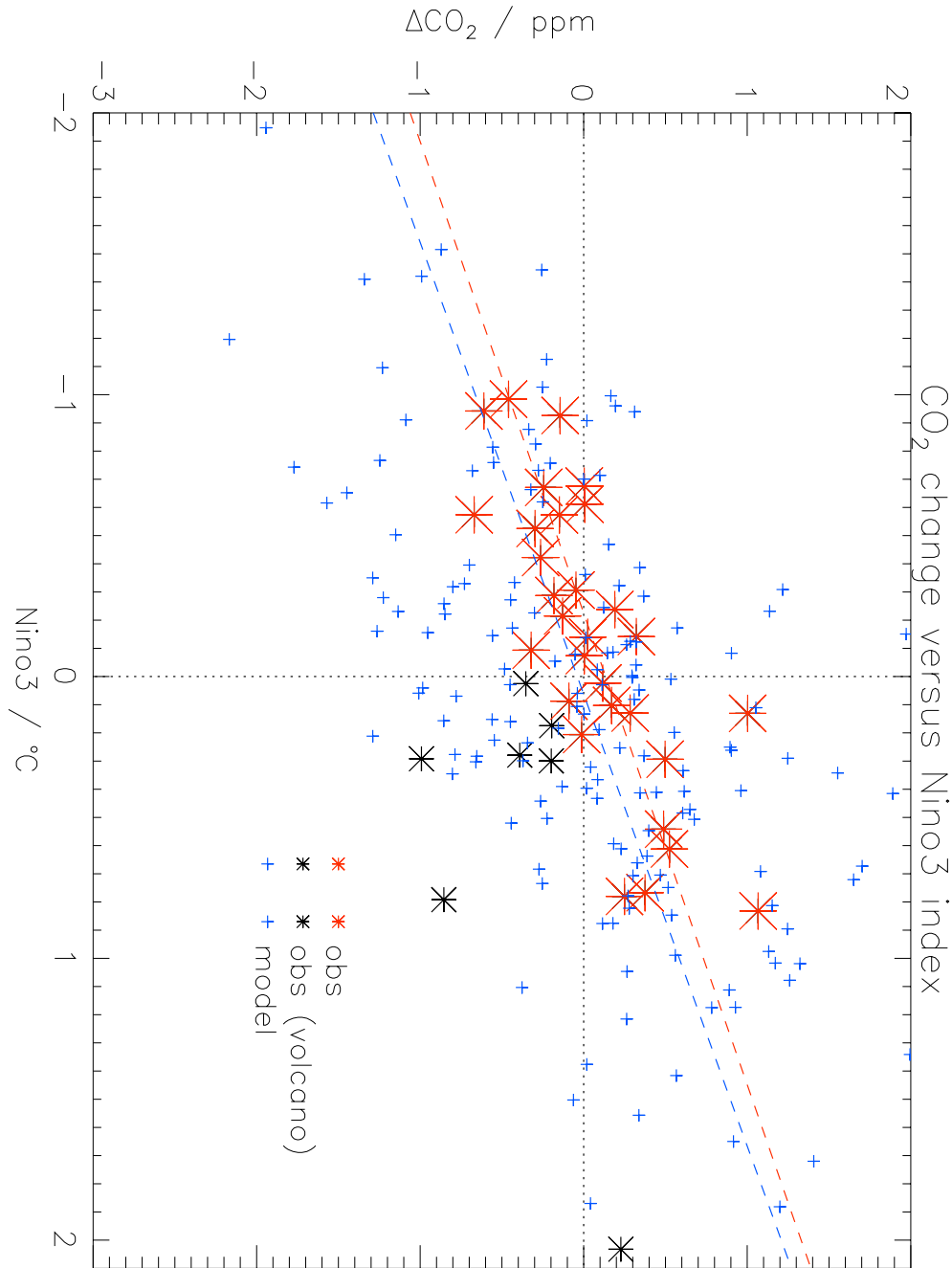


Figure 6: Anomaly in the growth rate of atmospheric CO_2 versus Nino 3 index (i.e. the annual mean sea-surface temperature anomaly in the tropical Pacific, 150°W - 90°W , 5°S - 5°N) from the pre-industrial control simulation (blue crosses) and the Mauna Loa observations (red stars). The gradients of the red dashed and blue dashed lines represent the sensitivity of the carbon cycle to ENSO, as given by the observations and the model respectively. We have excluded observations which immediately follow major volcanic events (black stars), since during these years the carbon cycle may have been significantly perturbed by the induced tropospheric cooling.

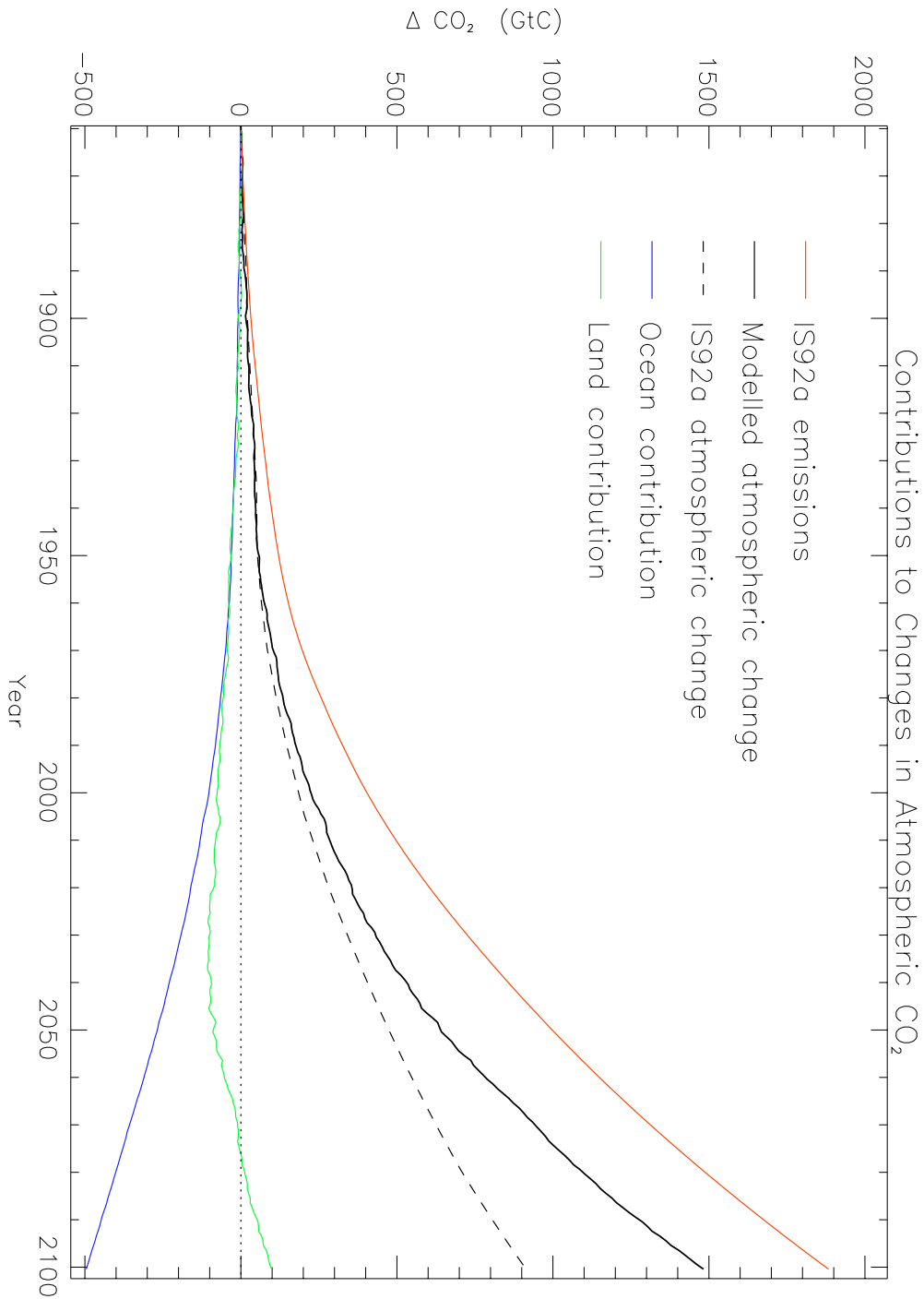


Figure 7: Budgets of carbon during the coupled climate-carbon cycle simulation. The continuous black line shows the simulated change in atmospheric CO₂ (in GtC). The red, green and blue lines show the integrated impact of the emissions, and of land and ocean fluxes respectively, with negative values implying net uptake of CO₂. For comparison the standard IS92a atmospheric CO₂ scenario is shown by the black dashed line. Note that the terrestrial biosphere takes up CO₂ at a reducing rate from about 2010 onwards, becoming a net source at around 2050.

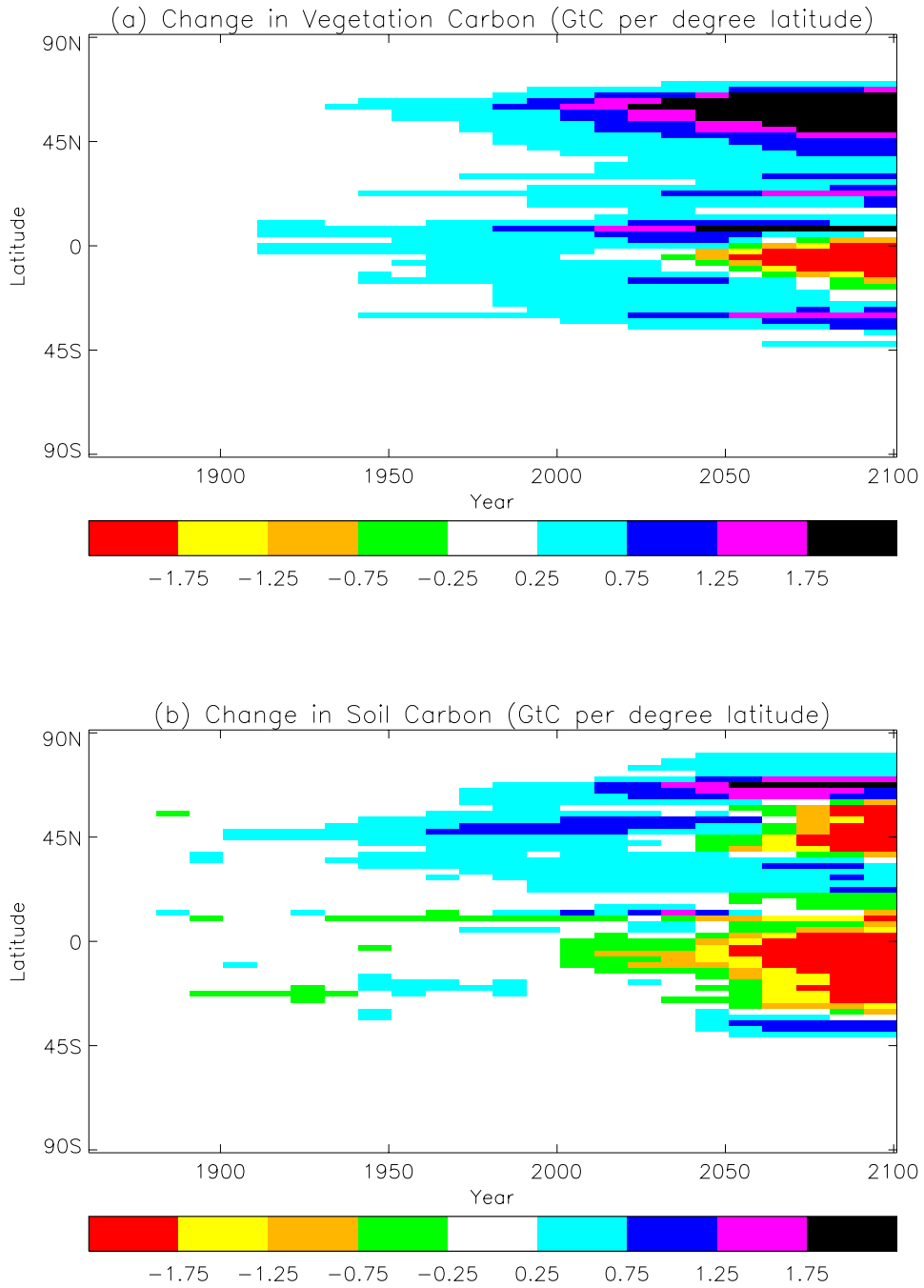


Figure 8: Latitude-time plot of modelled changes in vegetation carbon (a) and soil carbon (b) relative to 1860.

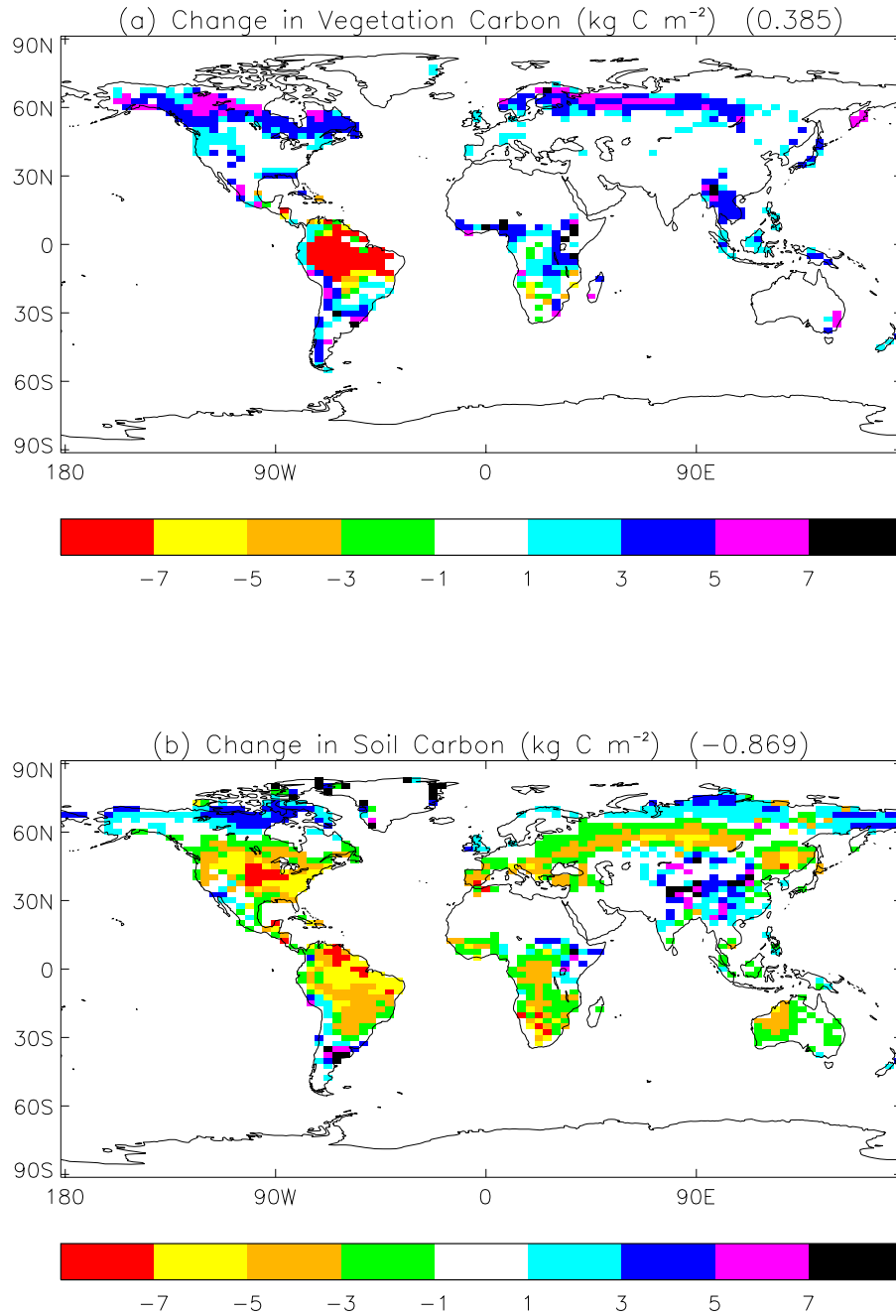


Figure 9: Modelled changes in vegetation carbon (a) and soil carbon (b) throughout the transient simulation (calculated as the difference between the mean for the 2090s minus the mean for the 1860s).

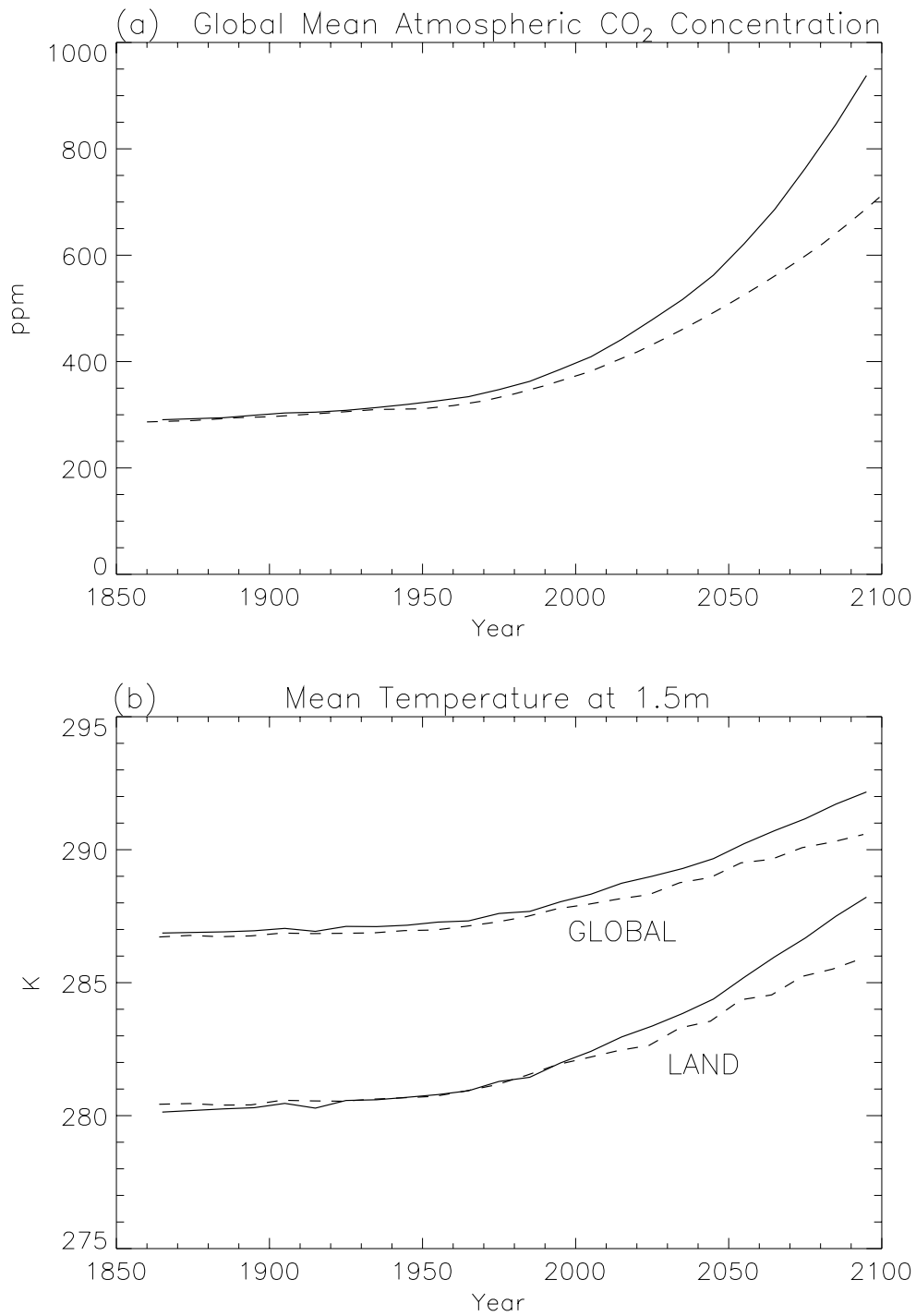


Figure 10: Comparison between the transient simulation with interactive CO₂ and dynamic vegetation (continuous lines), and the standard HadCM3 run with prescribed CO₂ and fixed vegetation (dashed lines). (a) Global mean CO₂ concentration and (b) global mean and land mean temperature, versus year.